

The Cannonball Model Of Long GRBs - Overview

Shlomo Dado and Arnon Dar

Physics Department, Technion, Haifa 32000, Israel

Abstract. During the past ten years, the predictions of the cannonball (CB) model of gamma ray bursts (GRBs) were repeatedly confronted with the mounting data from space- and ground-based observations of GRBs and their afterglows (AGs). The two underlying radiation mechanisms of the model, inverse Compton scattering (ICS) and synchrotron radiation (SR), provided an accurate description of the prompt and afterglow emission in all of the many well-sampled GRBs that were studied. Simple as they are, these two mechanisms and the burst environment were shown to generate the observed rich structure of the GRB light-curves at all observed frequencies and times.

Keywords: Gamma Ray Bursts, Inverse Compton Scattering, Synchrotron Radiation

PACS: 98.70.Rz

1. INTRODUCTION

Two models have been used extensively to analyze Gamma ray bursts (GRBs) and their afterglows (AGs): the fireball (FB) model and the cannonball (CB) model. Despite their similar names, the two models were and still are entirely different, hence only one of them, if either, may provide a faithful physical description of GRBs. Until recently, the fireball (FB) model has been widely accepted as that model. However, the rich and accurate data that have been accumulated in recent years from space- and ground-based observations have challenged this prevailing view on GRBs (for details see [1] and references therein): Synchrotron radiation (SR) cannot explain simultaneously their prompt optical emission and their hard X-ray and γ -ray emission. The prompt hard X-ray and γ -ray pulses cannot be explained by SR from internal shocks generated by collisions between conical shells. Neither can SR explain their typical energy, spectrum, spectral evolution, pulse-shape, rapid spectral softening during their fast decay phase and the established correlations between various observables. Moreover, contrary to the predictions of the FB model, the broadband afterglows of GRBs are highly chromatic at early times, the brightest GRBs do not show jet breaks, and in canonical GRBs where breaks are present, they are usually chromatic and do not satisfy the ‘closure relations’ expected from FB model ‘jet breaks’.

In spite of the above, the GRB community is not so critical and many authors believe that the GRB data require only some modifications of the standard FB model in order to accommodate the observations. Other authors simply ignore the failures of the FB model and continue the interpretation of the observations with the FB model taxonomy (‘colliding conical shells’, ‘internal and external shocks’, ‘forward and reverse shocks’, ‘continuous energy injection’, ‘refreshed shocks’) and parametrize the data with

freely adopted formulae (e.g., ‘segmented power laws’, ‘exponential-to power-law components’) which were never derived explicitly from any underlying physical assumptions (for recent examples, see, e.g. [2],[3],[4]).

The situation of the CB model is entirely different. In a series of publications, which were largely ignored by the rest of the GRB community, it was demonstrated repeatedly that the model correctly predicted the main observed properties of GRBs and reproduces successfully the diverse broad-band light-curves of both long GRBs ([1] and references therein) and short hard bursts (SHBs) [5]. Here we highlight this success of the CB model for long GRBs.

2. THE CB MODEL

In the CB model [6,7], *long-duration* GRBs and their AGs are produced by bipolar jets of highly relativistic plasmoids of ordinary matter [8,9] ejected in core-collapse supernova (SN) explosions [10]. It is hypothesized that an accretion disk or a torus is produced around the newly formed compact object, either by stellar material originally close to the surface of the imploding core and left behind by the explosion-generating outgoing shock, or by more distant stellar matter falling back after its passage [11]. As observed in microquasars, each time part of the accretion disk falls abruptly onto the compact object two jets of cannonballs (CBs) made of *ordinary-matter plasma* are emitted with large bulk-motion Lorentz factors in opposite directions along the rotation axis, from where matter has already fallen back onto the compact object due to lack of rotational support. The prompt γ -ray and X-ray emission is dominated by inverse Compton scattering (ICS) of photons of the SN glory - light scattered and/or emitted by the pre-supernova wind blown from the progenitor star. The CBs’ electrons Compton up-scatter the glory photons to γ and X-ray energies and collimate them into a narrow beam along the CBs’ directions of motion.

A second mechanism besides ICS that generates radiation by a CB is synchrotron radiation (SR). The emitted CBs, which initially expand in their rest frame with the speed of sound in a relativistic plasma, merge within a short (observer) time into a few leading CBs. The beamed radiation of the CBs ionizes the wind/ejecta blown by the progenitor star and the interstellar medium (ISM) in front of them. In the CBs’ rest frame, the ions continuously impinging on a CB generate within it a turbulent magnetic field, which is assumed to be in approximate energy equipartition with them. In this field the Fermi accelerated CB electrons and ISM intercepted electrons emit synchrotron radiation. The initial expansion of a CB produces a rapidly rising SR light-curve that begins to decline and traces the circumburst density of the pre-supernova wind/ejecta blown by the progenitor star into the roughly constant ISM density. Only when the CB has swept a mass comparable to its rest mass, does the continuous collision with the medium begin to decelerate it effectively. This results in a gradual steepening (break) of the SR light-curve into an asymptotic power-law decay.

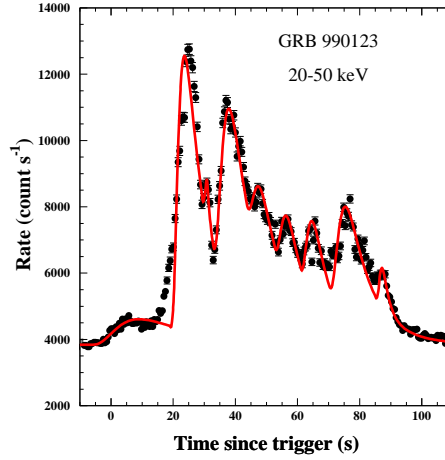


FIGURE 1. The BATSE light-curve of GRB 990123 and its CB model description [12]

3. PROMPT γ -RAY AND X-RAY EMISSION

3.1. The pulse shape and spectral evolution

A GRB is a sum of pulses beginning at different times. Let t denote the time after the beginning of such a pulse. Its light-curve produced by inverse Compton scattering of glory photons with a thin bremsstrahlung spectrum by the bulk of the CB's electrons which are comoving with it, is generally well approximated by [1]

$$E \frac{d^2 N_\gamma}{dt dE}(E, t) \approx A \frac{t^2 / \Delta^2}{(1 + t^2 / \Delta^2)^2} e^{-E/E_p(t)} \approx e^{-E/E_p(0)} F(E t^2), \quad (1)$$

where A is a constant that depends on the CB's baryon number, on its Lorentz and Doppler factors, on the density of the glory light and on the GRB's redshift and distance, and

$$E_p(t) \approx E_p(0) \frac{t_p^2}{t^2 + t_p^2}, \quad (2)$$

with t_p being the time when the ICS contribution to $E d^2 N_\gamma / dE dt$ reaches its peak value. It satisfies $E_p = E_p(t_p)$, where E_p is the peak energy of the time-integrated spectrum. Thus, in the CB model, each ICS pulse in the GRB light-curve is described by four parameters, A , $\Delta(E)$, $E_p(0)$ and the beginning time of the pulse which is set to be 0. Eq. (1), with E_p given by Eq. (2), describes well the shape and the spectral evolution of GRB pulses and of early-time X-ray flares. In particular, it correctly describes the rapid spectral softening during the fast decline phase of the prompt emission in GRBs and XRFs. This is demonstrated in Figs. 1 and 2 for the most energetic GRB with known redshift, 990123, and for the faint XRF 060218. If absorption in the CB is dominated by free-free absorption, then $\Delta(E) \propto E^{-0.5}$, and then for $E < E_p$ the light-curve of an ICS peak is approximately a function of $E t^2$ (the ' $E t^2$ ' law'), with a peak at $t = \Delta$, a

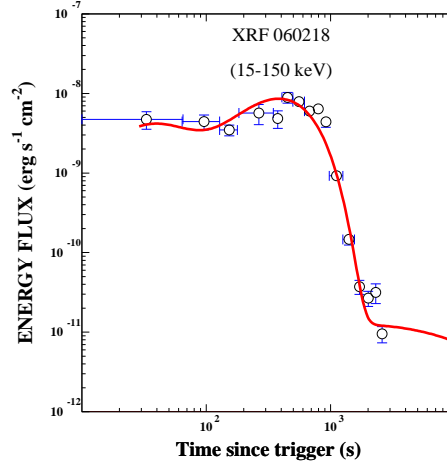


FIGURE 2. The Swift/BAT light-curve of XRF060218 and its CB model description [1]

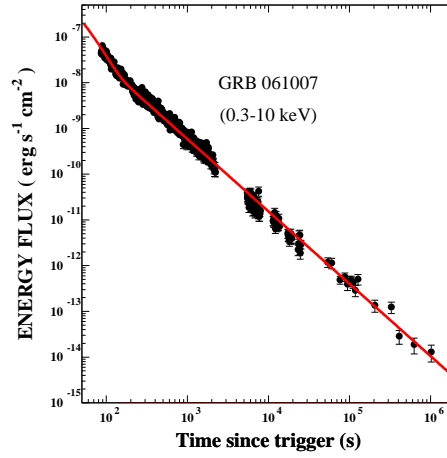


FIGURE 3. The Swift/XRT X-ray light-curve of GRB 061007, and its CB model description [1]. The prompt emission decays like t^{-2} .

full width at half maximum, $\text{FWHM} \approx 2\Delta$ and a rise time from half peak value to peak value, $\text{RT} \approx 0.30\text{FWHM}$.

Note that the temporal decay of the energy flux of the prompt emission within an energy band, which follows from Eqs. (1) and (2), is given approximately by,

$$\int_{E_1}^{E_2} E \frac{d^2 N_\gamma}{dt dE}(E, t) dE \approx A \frac{E_p(t) \Delta^2}{t^2} [e^{-E_1/E_p(t)} - e^{-E_2/E_p(t)}]. \quad (3)$$

Thus, for the Swift XRT light-curves where $E_1 = 0.3$ keV and $E_2 = 10$ keV, as long as $E_p(t) \gg E_2 \geq E_1$, the energy flux decays like t^{-2} until it is taken over by the SR afterglow, as demonstrated in Fig. 3 for the bright GRB 061007. If $E_1 \ll E_p(t)$ but

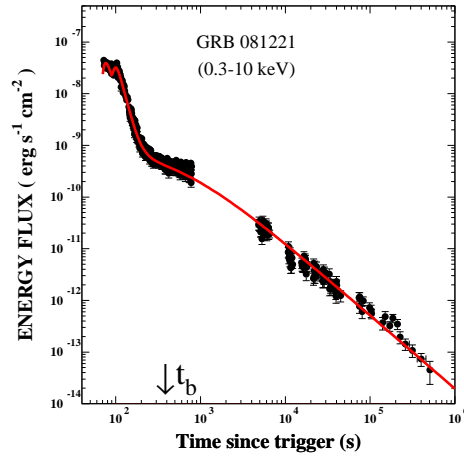


FIGURE 4. The Swift/XRT X-ray light-curve of GRB 081221 and its CB model description. The prompt emission decays like t^{-4} .

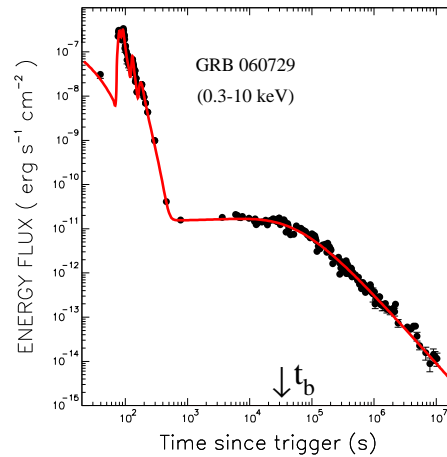


FIGURE 5. The Swift/XRT light-curve of GRB 060729 and its CB model description [1]. The prompt emission pulses decay like t^{-4} times a Gaussian.

$E2 \gtrsim E_p(t)$ the energy flux decays like t^{-4} , until it is taken over by the SR afterglow, as demonstrated in Fig. 4 for GRB 081221. When $E1 \gtrsim E_p(t)$ then the energy flux of the prompt emission decays like $t^{-4} e^{-Et^2/2E_p t_p^2}$ until it is taken over by the SR afterglow, as shown in Fig. 5. .

3.2. Polarization of the prompt emission

The ICS of external unpolarized light by a highly relativistic and narrowly collimated jet of CBs results in a polarization of the hard X-ray and γ -ray emission that is given approximately by [8,6],

$$\Pi(\theta, \gamma) \approx \frac{2\theta^2\gamma^2}{1+\theta^4\gamma^4}, \quad (4)$$

which, for the most probable viewing angles, $\theta \approx 1/\gamma$, is of $\mathcal{O}(100\%)$. The polarization of the prompt γ -ray emission has been measured in four GRBs [13-16] where a linear polarization $\Pi = (80 \pm 20)\%$ in GRB 021206, $35\% \leq \Pi \leq 100\%$ in GRB 930131, $50\% \leq \Pi \leq 100\%$ in GRB 960924 and $\Pi = 98\% \pm 33\%$ in GRB 041219A were obtained. Subsequent analyses of the case of GRB 021206 by other groups questioned the result at the same level of significance [17,18], so that the degree of polarization of GRB 021206 remained uncertain.

3.3. Correlations between the prompt emission observables

The relativistic boosting and beaming of the glory photons by a CB yield the relations [6,19] $E_{iso} \propto \delta^3$, $(1+z)^2 L_p \propto \delta^4$, $(1+z)E_p \propto \gamma\delta$, and $E_p \propto 1/\Delta$, where E_{iso} is the isotropic equivalent gamma ray energy, L_p is the peak isotropic equivalent luminosity, γ is the bulk motion Lorentz factor of a CB, and $\delta = 1/\gamma(1-\beta \cos\theta)$ is its Doppler factor with θ being the angle between the line of sight to the CB and its direction of motion. For $\gamma^2 \gg 1$ and $\theta^2 \ll 1$, $\delta \approx 2\gamma/(1+\gamma^2\theta^2)$ to an excellent approximation. The strong dependence of observables such as E_{iso} , L_p , E_p and Δt on γ and δ and the narrow distribution of θ around $1/\gamma$ result in correlations among them [19] that are roughly represented by an average power-law,

$$(1+z)E_p \propto E_{iso}^{0.50 \pm 0.17} \propto [(1+z)^2 L_p]^{0.375 \pm 0.125}; \quad \Delta t \propto 1/E_p. \quad (5)$$

The observed correlations between $(1+z)E_p$ and E_{iso} in GRBs with known redshift, E_p and fluence are compared in Fig. 6 with that predicted in the CB model [19, 20]. As shown in Fig. 6, the CB model correctly predicted the observed correlation, e.g., [21,22], between $(1+z)E_p$ and E_{iso} .

4. SYNCHROTRON RADIATION

The ISM ions continuously impinging on a CB with a relative Lorentz factor $\gamma(t)$ generate within it an equipartition turbulent magnetic field. In this field the intercepted electrons emit isotropic synchrotron radiation with a characteristic frequency, $\nu'_b(t)$, which is Doppler boosted and collimated by its relativistic motion. In the observer's frame:

$$\nu_b(t) \simeq \frac{\nu_0}{1+z} \frac{[\gamma(t)]^3 \delta(t)}{10^{12}} \left[\frac{n}{10^{-2} \text{ cm}^3} \right]^{1/2} \text{ Hz}, \quad (6)$$

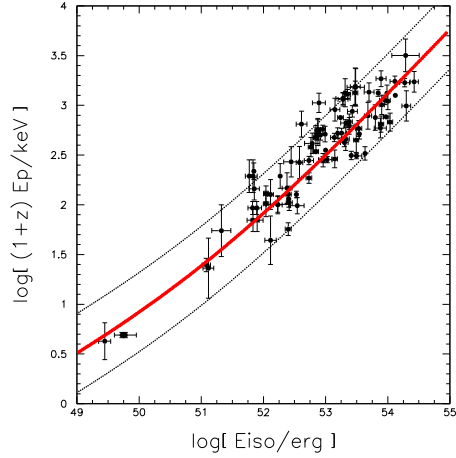


FIGURE 6. The observed correlation between $(1+z)E_p$ and E_{iso} and that predicted by the CB model [19,20] for long GRBs before 2009, with reliable z , E_p and E_{iso} values

where $\nu_0 \simeq 3.85 \times 10^{16} \text{ Hz} \simeq 160 \text{ eV/h}$. The spectral energy density of the SR from a single CB at a luminosity distance D_L is given by [7]:

$$F_\nu \simeq \frac{\eta \pi R^2 n m_e c^3 \gamma(t)^2 \delta(t)^4 A(\nu, t)}{4 \pi D_L^2 \nu_b(t)} \frac{p-2}{p-1} \left[\frac{\nu}{\nu_b(t)} \right]^{-1/2} \left[1 + \frac{\nu}{\nu_b(t)} \right]^{-(p-1)/2}, \quad (7)$$

where $p \sim 2.2$ is the typical spectral index of the Fermi accelerated electrons, $\eta \approx 1$ is the fraction of the energy of the intercepted electrons that is synchrotron re-radiated, and $A(\nu, t)$ is the attenuation of photons of observed frequency ν along the line of sight through the CB, the host galaxy (HG), the intergalactic medium (IGM) and the Milky Way (MW):

$$A(\nu, t) = \exp[-\tau_\nu(\text{CB}) - \tau_\nu(\text{HG}) - \tau_\nu(\text{IGM}) - \tau_\nu(\text{MW})]. \quad (8)$$

The opacity $\tau_\nu(\text{CB})$ at very early times, during the fast-expansion phase of the CB, may strongly depend on time and frequency. The opacity of the circumburst medium [$\tau_\nu(\text{HG})$ at early times] is affected by the GRB and could also be t - and ν -dependent. The opacities $\tau_\nu(\text{HG})$ and $\tau_\nu(\text{IGM})$ should be functions of t and ν , for the line of sight to the CBs varies during the AG observations, due to the hyperluminal motion of CBs.

The diverse behaviour of the broadband SR emission in GRBs is well described by Eq. (7) [1]. Due to lack of space we shall discuss only two of its important limits.

4.1. The early-time SR

The scattering of the wind's particles by the CB stops its initial rapid expansion within a short time $t = t_{exp}$ [7]. During that time both γ and δ stay put at their initial values and

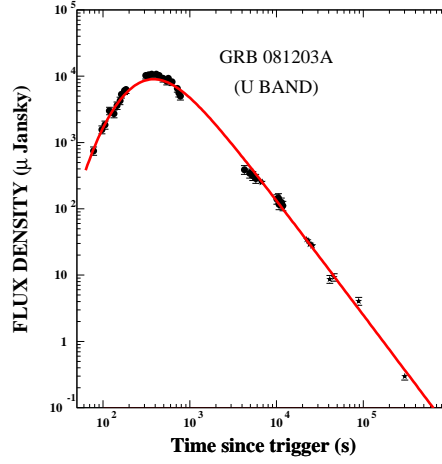


FIGURE 7. The U -band light-curve of GRB 080319B [3] and its CB model description

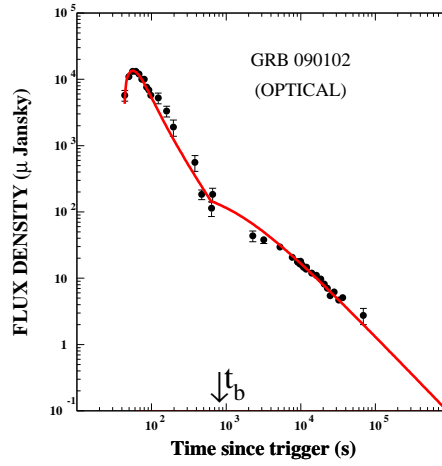


FIGURE 8. The R -band light-curve of GRB 090102 and its CB model description

Eq. (7) reduces to the early-time limit [1],

$$F_\nu \propto \frac{e^{-a/t} t^{1-\beta}}{t^2 + t_{exp}^2} \nu^{-\beta}, \quad (9)$$

where $\beta(t) = 0.5$ for $\nu \ll \nu_b(t)$ and $\beta(t) = p/2$ for $\nu \gg \nu_b(t)$. Figs. 7 and 8 compare this prediction with the observed prompt optical emission in GRBs 081203A [25] and 090102 [26], while Fig. 9 compares them for the brightest observed GRB, 080319B [3], where the prompt optical emission is resolved into contributions of 3 CBs (or a single CB crossing a wind blown with interruptions).

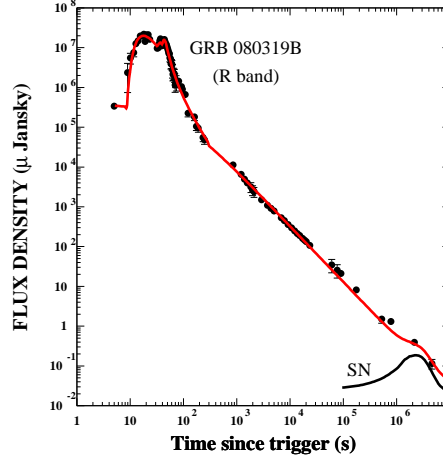


FIGURE 9. Comparison between the optical light-curve of GRB 080319B and that predicted by the CB model [12]

4.2. SR during the CB's coasting phase

The continuous collision with the medium decelerates the CB. When the CB enters the constant density ISM, relativistic energy-momentum conservation yields the deceleration law ([1] and references therein):

$$\gamma(t) = \frac{\gamma_0}{\sqrt{[(1 + \theta^2 \gamma_0^2)^2 + t/t_0]^{1/2} - \theta^2 \gamma_0^2}}, \quad (10)$$

with $t_0 = (1+z)N_B/8cn\pi R^2\gamma_0^3$. As can be seen from Eq. (10), γ and δ change little as long as $t \ll t_b = [1 + \gamma_0^2 \theta^2]^2 t_0$, and Eq. (7) yields the ‘plateau’ of canonical AGs. For $t \gg t_b$, γ and δ decrease like $t^{-1/4}$. The transition $\gamma \sim \gamma_0$ to $\gamma \sim \gamma_0 (t/t_0)^{-1/4}$ around t_b induces a bend, the so-called ‘jet break’, in the synchrotron AG from a plateau to an asymptotic power-law $F_\nu \propto t^{-p/2-1/2} \nu^{-p/2} = t^{-\Gamma+1/2} \nu^{-\Gamma+1}$. In terms of the frequently used notation, this asymptotic behaviour satisfies $F_\nu(t) \propto t^{-\alpha} \nu^{-\beta}$ with $\alpha = \beta + 1/2 = \Gamma - 1/2$. For a density $n \propto 1/r^2$, the asymptotic relation becomes $\alpha = \beta + 1 = \Gamma$, where t is the time after the onset of the $n \propto 1/r^2$ density. These relations are well satisfied by the late-time power-law decay of canonical and non-canonical AGs and of late-time SR flares [1,23].

4.3. Jet breaks and ‘missing breaks’

In terms of typical CB-model values of γ_0 , R , N_B and n ,

$$t_b = (1300\text{s}) [1 + \gamma_0^2 \theta^2]^2 (1+z) \left[\frac{\gamma_0}{10^3} \right]^{-3} \left[\frac{n}{10^{-2} \text{cm}^{-3}} \right]^{-1} \left[\frac{R}{10^{14} \text{cm}} \right]^{-2} \left[\frac{N_B}{10^{50}} \right]. \quad (11)$$

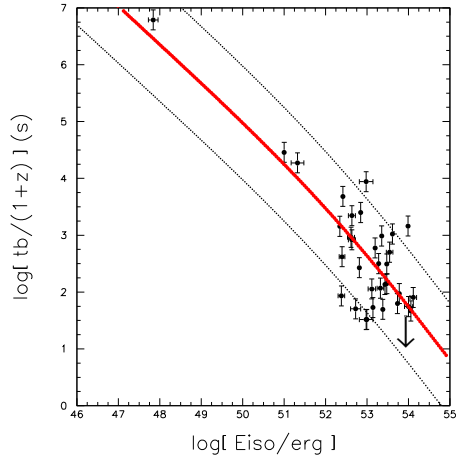


FIGURE 10. The observed correlation between $t_b/(1+z)$ and E_{iso} for long GRBs with well measured redshift and E_{iso} and that predicted by the CB model [23]

Consequently, for a large density, a large γ_0 and a small viewing angle, which correspond to large values of E_{iso} , L_p and E_p , the break time t_b becomes very small and may ‘hide’ under the prompt ICS radiation, or occur too early to be seen by the Swift XRT [23]. In that case the X-ray AG measured by Swift XRT has the simple asymptotic power-law decay, $F_\nu(t) \propto t^{-\beta x - 1/2} \nu^{-\beta x}$, as was observed for several GRBs such as 050717, 061007, 071025, 080319B, 080804 and 081109 (see e.g., Fig. 3).

5. BREAK TIME - PROMPT EMISSION CORRELATIONS

For a constant ISM density, $t_b/(1+z) \propto 1/\gamma_0 \delta_0^2$. Consequently, the favoured viewing angle $\theta \approx 1/\gamma_0$, i.e., $\delta_0 \approx \gamma_0$, and Eq. (5) imply correlations roughly represented by [23] $t_b/(1+z) \propto E_{iso}^{-1}$, $t_b/(1+z) \propto [(1+z) E_p]^{3/2}$, etc., while for large viewing angles the strong dependence on δ_0 yields $t_b/(1+z) \propto E_{iso}^{-2/3}$ and $t_b/(1+z) \propto [(1+z) E_p]^2$, etc. These limits can be well interpolated by formulae such as,

$$\frac{t_b}{1+z} \approx \frac{2 t_{b,eiso}}{(E_{iso}/E_0)^{2/3} + E_{iso}/E_0} \sim t_{b,eiso} \left(\frac{E_{iso}}{E_0} \right)^{-0.83 \pm 0.17}. \quad (12)$$

The predicted correlation between t_b and E_{iso} is compared in Fig. 10 to data on Swift GRBs prior to January 1, 2009 that have a well measured E_{iso} and a well sampled X-ray light-curve. The explanation for ‘missing AG breaks’ is supported by the observed correlations between the break-time and the prompt emission observables [23].

6. FLARES

In more than 50% of the GRBs observed by Swift, the X-ray light-curve, during the prompt GRB and its early AG phase, shows flares superimposed on a smooth background. In the CB model, X-ray flares without an accompanying detectable γ -ray emission can be of two kinds. They can be ICS flares produced by CBs ejected with a relatively small Lorentz factor and/or a large viewing angle. Such CBs may be ejected in accretion episodes both during the prompt GRB and in delayed accretion episodes onto the newly formed central object in core collapse SNe [11]. ICS flares satisfy the $E t^2$ -law and exhibit a rapid softening during their fast decline phase that is well described by Eqs. (1) and (2). Often, during the rapidly decreasing phase of the prompt emission, there are ‘mini X-ray flares’ that show this rapid spectral softening [24]. As the accretion material is consumed, one may expect the ‘engine’ to have a few progressively-weakening dying pangs. Flares can also result from enhanced synchrotron emission during the passage of CBs through over-densities produced by mass ejections from the progenitor star or by interstellar winds [7]. Late flares seem to have the typical SR spectrum and spectral evolution induced by the dependence of v_b on density.

7. CONCLUSION

The widely ignored CB model continues to be a remarkably successful model of GRBs.

REFERENCES

1. S. Dado, A. Dar and A. De Rújula, *ApJ*, in press (2009), arXiv:0809.4776
2. J. S. Bloom, et al. *ApJ*, in press (2009), arXiv:0803.3215
3. J. L. Racusin et al. *Nature*, **455**, 183-188 (2008), arXiv:0805.1557
4. K. L. Page, et al. *MNRAS*, in press (2009), arXiv:0901.2219
5. S. Dado and A. Dar, *ApJ*, in press (2009), arXiv:0807.1962
6. A. Dar and A. De Rújula, *Phys. Rep.*, **405**, 203-278 (2004), arXiv:astro-ph/0308248
7. S. Dado, A. Dar and A. De Rújula, *A&A*, **388**, 1079-1105 (2002), arXiv:astro-ph/0107367
8. N. Shaviv and A. Dar, *ApJ*, **447**, 863-873 (1995), arXiv:astro-ph/9407039
9. A. Dar, *ApJ*, **500**, L93-L96 (1998), arXiv:astro-ph/9709231
10. A. Dar and R. Plaga, *A&A*, **349**, 259-266 (1999), arXiv:astro-ph/9902138
11. A. De Rújula, *PL*, **193**, 514-517 (1987)
12. S. Dado and A. Dar, *ApJ*, 2008, arXiv:0812.3340
13. W. Coburn, and S. E. Boggs, *Nature*, **423**, 415-417 (2003), arXiv:astro-ph/0305377
14. D. R. Willis, et al. 2005, *A&A*, **439**, 245-253 (2005), arXiv:astro-ph/0505097
15. E. Kalemci, E., et al. 2007, *ApJS*, **169**, 75-82 (2007)
16. S. McGlynn, et al. *A&A*, **466**, 895-904 (2007), arXiv:astro-ph/0702738
17. R. E. Rutledge and D. E. Fox, *MNRAS*, **350**, 1288-1300 (2004), arXiv:astro-ph/0310385
18. C. Wigger, et al. *ApJ*, **613**, 1088-1100 (2004), arXiv:astro-ph/0405525
19. A. Dar and A. De Rújula, (2000), arXiv: astro-ph/0008474
20. S. Dado, A. Dar and A. De Rújula, *ApJ*, **663**, 400-406 (2007), arXiv:astro-ph/0701031
21. L. Amati, et al. *A&A*, **390**, 81-89 (2002), arXiv:astro-ph/0205230
22. L. Amati, 2008, *MNRAS*, **391**, 577-584 (2008), arXiv:0805.0377
23. S. Dado, A. Dar and A. De Rújula, *ApJ*, **680**, 517-530 (2008), arXiv:0712.1527
24. S. Dado, A. Dar and A. De Rújula, *ApJ*, **681**, 1408-1418 (2008), arXiv:0709.4307
25. N. P. M. Kuin, et al. (2008), arXiv:0812.2943